Chimia 48 (1994) 397–400

ISSN 0009–4293

Picosecond Transient Grating Spectroscopy: an Application of Holography for Investigating Ultrafast Photoinduced Processes

Eric Vauthey*, **Yvan Pariat**, and **Arthur Henseler**

Abstract. The principles of ps transient grating spectroscopy are presented. The capabilities of this technique for the study of photoinduced processes are illustrated by several new results. These include the observation of an anomalous effect in the reorientation dynamics of two ionic dyes in long-chain alkanenitriles, the measurement of the local viscosity in the interior of reverse micelles containing methanol, and the determination of the rate constant of separation of a geminate radical pair formed by photoinduced electron-transfer reaction.

1. Introduction

If flash photolysis can be considered to be a special application of photography, transient grating spectroscopy is its holographic counterpart. While, in flash photolysis, one records the amplitude changes of a probing light beam, in transient grating spectroscopy, the information is contained in both the phase and the amplitude of the diffracted probe beam.

The use of holography to study photochemical and photophysical processes was introduced in the 80's by *Bräuchle* and *Burland* [1]. This method using cw lasers has proven to be well suited to investigate slow processes in solids [2]. Transient grating spectroscopy is predominantly used in solid state physics [3], but it has been applied by *Fayer* and co-workers to investigate photophysical processes in solids, liquids, and flames [4]. In this paper, we describe several new results to illustrate how ps transient grating spectroscopy can be a valuable and powerful alternative to the now classical flash-photolysis technique.

2. Principles of Transient Grating Spectroscopy

In a transient experiment, the sample is excited by two spatially crossed and time-coincident laser pulses producing an interference pattern (*Fig. 1a*). This spatially modulated excitation creates in the sample spatial distributions of ground state, excited state, and/or photochemical intermediate and product populations. Consequently, similar modulations of the refractive index and absorbance are generated. The amplitude of these grating-like distributions can be measured by a third, time-delayed laser pulse striking the grating at *Bragg* angle (*Fig. 1b*). The relationship between the diffracted intensity and the amplitude of the modulations at the probing wavelength can be calculated by the following equation proposed by *Kogelnik* for a plane-wave hologram [5]:

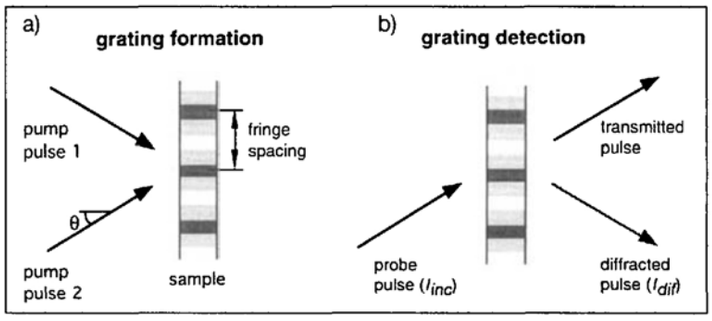

Fig. 1. *Schematic illustration of the principle of transient grating spectroscopy*

$$\frac{I_{dif}}{I_{inc}} = \left[\sin^2\left(\frac{\pi n_1 d}{\lambda \cos\theta}\right) + \sinh^2\left(\frac{\alpha_1 d}{2\cos\theta}\right)\right] \cdot \exp\left(-\frac{2\alpha_0 d}{\cos\theta}\right) \quad (1)$$

where I_{dif} and I_{inc} are the diffracted and incident light intensities, respectively, d the optical path length, n_1 and α_1 the modulation amplitudes of refractive index and absorbance gratings at the probing wavelength λ, θ the *Bragg* angle and α_0 the average absorbance of the sample at λ. The first term in the square brackets describes the modulation of the refractive index, the phase grating. The second term is related to the modulation of absorbance, the amplitude grating. The exponential term accounts for the unmodulated absorption of the sample. If the probing wavelength is close to the absorption maximum of the monitored species, n_1 goes to zero and the contribution of the phase grating can be neglected. In this case and for small I_{dif}/I_{inc} ratios, *Eqn. 1* can be simplified to:

$$\frac{I_{dif}}{I_{inc}} = \left(\frac{\alpha_1 d}{2\cos\theta}\right)^2 \cdot \exp\left(-\frac{2\alpha_0 d}{\cos\theta}\right) \quad (2)$$

The modulation amplitude α_1 depends directly on the concentration changes, ΔC of each component i with an extinction coefficient ε:

$$\alpha_1(\lambda) = \sum_i \varepsilon_i(\lambda)\Delta C_i \quad (3)$$

These last two equations indicate that the intensity of the diffracted signal is proportional to the square of the concentration changes in the sample. Therefore, the kinetics of any population can be determined by monitoring the diffraction intensity at the corresponding wavelength as a function of the time delay between the two pump and the probe pulses.

This technique is a zero background detection method, contrarily to flash photolysis, where a small variation of light

*Correspondence: Dr. Eric Vauthey
Institut de Chimie Physique
Université de Fribourg
Pérolles
CH–1700 Fribourg

intensity has to be detected over a relatively intense light beam. For this reason, a few tens of μJ of pump energy are enough to create a detectable transient grating, minimizing the risk of sample degradation and the occurrence of optical nonlinear phenomena. Moreover, as the diffracted signal keeps the propagation characteristics of the probe beam, it can easily be isolated from fluorescence or scatter of the sample.

Transient grating spectroscopy can also be described within the framework of nonlinear optics as a four-wave-mixing process, where the square of the modulation amplitude can be considered as a component of the third-order nonlinear susceptibility, and the *Bragg* condition is equivalent to the phase-matching condition [6].

3. Experimental Setup

The transient grating setup is depicted in *Fig. 2*. A single pulse of the output train of a passively mode-locked Q-switched Nd:YAG laser (*Lumonics PML*) is frequency doubled after two passes in an amplifier (*Continuum SF 611-07*). 10% of the 532-nm output is sent along a fixed optical delay line and then split into two components of 70 and 30% intensity which are brought into interference on the sample cell. To ensure perfect time coincidence between the two pump pulses, the 30% component is deviated along a short adjustable optical delay line. For ground-state recovery measurements, a small fraction of the 532-nm laser output is sent along a variable optical delay line consisting of a retroreflector mounted on a motorised translation stage. The polarisation of this beam is controlled by a *Lyot* filter combined with a *Glan-Taylor* prism polariser. The probe beam has a counter-propagating direction relative to one of the pump beams and the diffracted beam has a counter-propagating direction relative to the other pump beam. Half of the diffracted signal is reflected by a beamsplitter into a vacuum photodiode. For measurements with the dye laser, 90% of the 532-nm output is used to pump a short cavity dye laser operating with *Rhodamine 590* and an amplification cell filled with *Kiton Red* (*Continuum PD10*). The dye laser pulses are sent along the motorised delay line as described above. The duration of the 532-nm and dye laser pulses are *ca.* 30 ps and less than 10 ps, respectively. The total pump intensity on the sample is *ca.* 5 mJ/cm^2, and the probe pulse intensity is *ca.* 10 times smaller. The photodiode signal is then amplified and fed into a PC-based multichannel analyser board (*Canberra Accuspec Nal*) for pulse-height analysis. The pulse energy of a fraction of one of the pump beams is measured with a photomultiplier tube. Its output signal is sent into a discriminator whose levels are set so that only laser pulses within a small energy range can generate a signal opening the gate of the multichannel analyser board. At each position of the delay line, the diffracted intensity is averaged over 200 laser pulses.

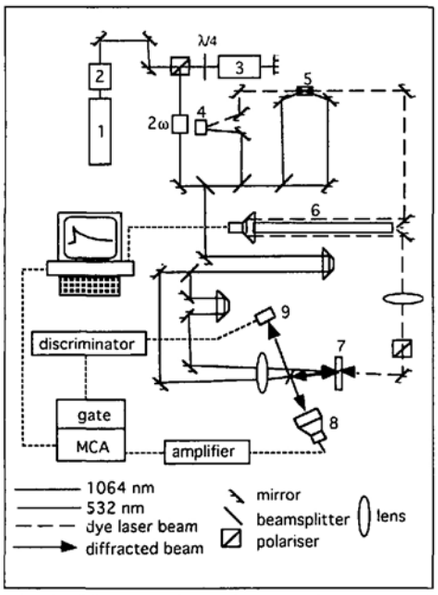

Fig. 2. *Picosecond transient grating set-up:* 1. *passively mode-locked Q-switched Nd:YAG laser,* 2. *single pulse selector,* 3. *Nd:YAG amplifier,* 4. *short cavity dye laser,* 5. *dye laser amplifier,* 6. *motorised optical delay,* 7. *sample,* 8. *vacuum photodiode,* 9. *photomultiplier tube*

4. Results and Discussion

4.1. *Molecular Reorientation Dynamics in Solution*

The rotational reorientation time of a solute molecule, τ_{rot}, can be obtained by combining the diffracted intensities measured with a probe light polarised parallel, $I^{\parallel}_{dif}(t)$, and perpendicular, $I^{\perp}_{dif}(t)$, to the polarisation of the pump light [7]:

$$r(t) = \frac{\left[I^{\parallel}_{dif}(t)\right]^{1/2} - \left[I^{\perp}_{dif}(t)\right]^{1/2}}{\left[I^{\parallel}_{dif}(t)\right]^{1/2} + 2\left[I^{\perp}_{dif}(t)\right]^{1/2}} = r_0 \cdot \exp\left(-\frac{t}{\tau_{rot}}\right) \quad (4)$$

where $r(t)$ is the polarisation anisotropy, r_0 being the initial anisotropy which amounts to 0.4 when the transition dipole involved in the probing process is parallel to that involved in the pumping stage. Depending on the wavelength of the probe pulses, the rotational dynamics of the molecule in different electronic states can be investigated. *Fig. 3* shows $I^{\parallel}_{dif}(t)$ and $I^{\perp}_{dif}(t)$ measured with rose Bengal in the ground state in butyronitrile, the insert being the polarisation anisotropy decay as calculated from *Eqn. 4*.

The rotational diffusion time of a molecule can reveal important information on its environment and on its interaction with the solvent. *Fig. 4* shows the rotational diffusion time of the ionic dyes rose Bengal and *Rhodamine 6G* in the ground state in a series of polar solvents of increasing viscosity. The solid lines have been calculated according to the *Stokes-Einstein-Debye* hydrodynamic theory, which predicts a linear relationship between τ_{rot} and viscosity. In long alkanenitriles, the rotation times deviate substantially from the theoretical predictions. This effect had previously been measured with Nile red, a neutral but polar molecule [8]. The long alkanenitriles are composed of a strongly polar and hydrophilic end and of an almost non-polar hydrophobic end, and they are, therefore, similar to surfactant molecules. The ionic dyes are only soluble in polar solvents, while Nile red is also slightly soluble in non-polar solvents. As all these dyes can be dissolved even in the longer alkanenitriles, the structure of the solvation layer must be similar to the structure of a reverse micelle. The polar or charged solute is predominantly surrounded by the CN group of the solvent, while the alkyl chain points away. With such a micelle-like structure, the movements of individual solvent molecules are more restricted than in the case of small solvent molecules like MeCN around a polar solute. Therefore, friction can be expected to be substantially larger than in a normal solvation layer. Consequently, the microviscosity around the solute molecule is larger than the macroscopic viscosity. To account for the discrepancy between normal and anomalous polar solvents, the local viscosity of valeronitrile and hexanenitrile around the solute molecule should be *ca.* 1.4 times larger than the macroscopic viscosity. In octanenitrile, the local viscosity should increase by a factor of 1.9. These values are very reasonable considering that this micellisation effect should increase with the length of the alkyl chain.

4.2. *Nonradiative Decay of a Cyanine in Reverse Micelles*

Once excited to the first singlet state, cyanine dyes are known to relax very rapidly to the ground state through a nonradiative decay coupled to *cis/trans*-isomerization. Experimental studies have shown that the excited lifetime is proportional to a fractional power of viscosity, $\tau \alpha \eta^{\alpha}$, where α can vary form 0.1 to 1 depending on the system [9]. Theoretically, this behavior has been explained with a model where the effect of solvent friction depends on the frequency of the potential barrier [10][11].

This dependence has been used to determine the local viscosity of the interior of reverse micelles of various sizes. A reverse micelle is usually composed of water surrounded by the surfactant in a non-polar solvent [12]. We have studied different types of reverse micelles in heptane with *Aerosol OT* (sodium bis(2-ethylhexyl)sulfosuccinate) as surfactant and in which water is replaced by MeOH. The microviscosity in the micelle was determined from the ground state recovery time of a cyanine dye, diethyl-3,3'-thiacarbocyanine iodide (DTCI), dissolved in the polar solvent pool. The lifetime to microviscosity relationship was calibrated with the recovery time of DTCI in reverse micelles containing water, whose microviscosity is known [13]. The measured recovery times are listed in the *Table* as a function of the polar solvent to surfactant molar ratio, R. It can be seen that the viscosity experienced by DTCI decreases strongly as R increases. This is due to an increase of the size of the polar solvent pool. The radius of the water pool within *Aerosol OT*, r_{wp}, has been experimentally found to be proportional to R: $r_{wp}=1.5\times R$ [14]. The *Table* shows that, for the same R value, the microviscosity is smaller in the MeOH than in the water pool. This difference can originate from two effects:

1) As a MeOH molecule is more than twice as large as a H_2O molecule, the size of the MeOH pool must be larger than that of the water pool for the same R value. Therefore, the dye molecule, whose shape can be approximated to an oblate spheroid with a long axis of 15 Å and a short axis of 6 Å, can move more freely.

2) H_2O is a better H-bonding solvent than MeOH, and, therefore, coupling between the dye and the charged head of the surfactant through solvent molecules could be more important in H_2O.

Similar measurements with non H-bonding polar solvents as MeCN are in progress.

These results show that the knowledge of the structure and viscosity of the interior of these reverse micelles is of primary importance in view of their application as microreactors [14].

4.3. *Dynamics of Photoinduced Electron-Transfer Reactions*

An important step in intermolecular photoinduced electron-transfer (e.t.) reactions is the separation of the geminate ion pair into free ions with a rate constant k_{sep}. A direct determination of this rate has recently been shown to be possible with

Table. *Ground-State Recovery Time, τ_{gsr}, of DTCI in* Aerosol OT *Reverse Micelles in Heptane, Microviscosity, η, and Water Pool Radius, r_{wp}, as a Function of the Polar Solvent to Surfactant Molar Ratio,* R. The microviscosity values in water pools are taken from [12].

Polar solvent	R	r_{wp} [Å]	τ_{gsr} [ps]	η [cP]
H_2O	4.1	6.1	940	62
H_2O	9.3	14	676	24
H_2O	16.4	25	650	20
H_2O	26.0	39	516	15
MeOH	0.0		966	67
MeOH	1.6		930	59
MeOH	4.1		620	17
MeOH	8.2		540	11
MeOH	∞		140	0.55

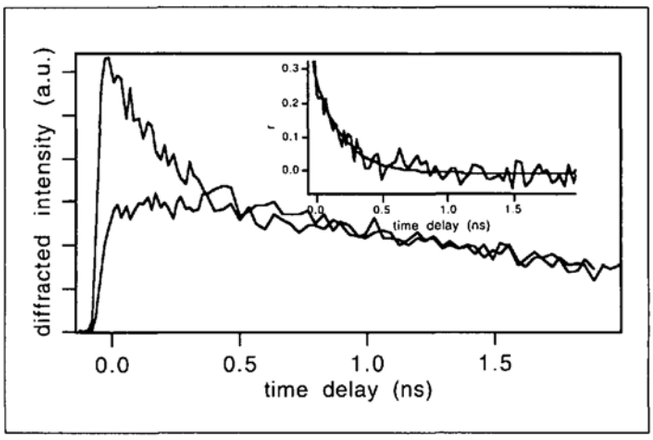

Fig. 3. *Time evolution of the diffracted intensity measured with probe pulses at 532 nm polarised parallel* (upper trace) *and perpendicular* (lower trace) *to the pump pulses with rose Bengal in butyronitrile at 293 K.* Insert: decay of the polarisation anisotropy with the same system and best single exponential fit (solid line).

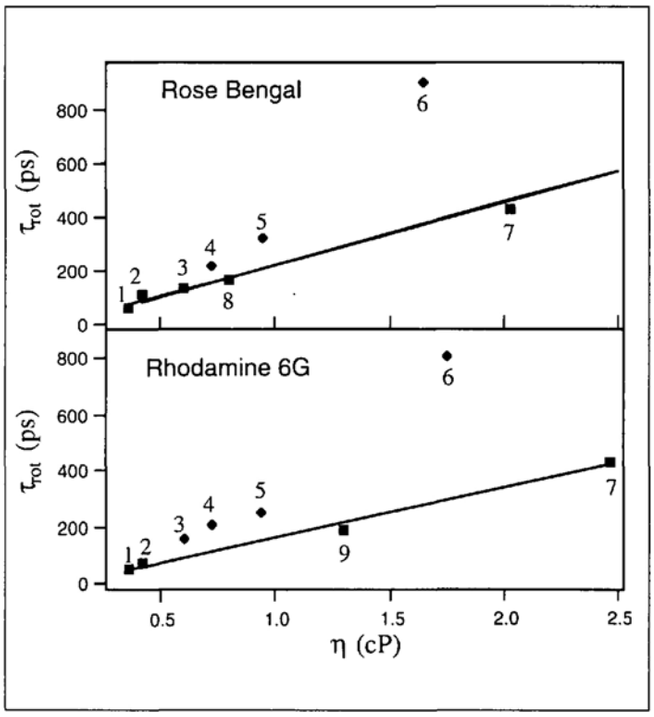

Fig. 4. *Rotational diffusion time of rose Bengal and* Rhodamine 6G *at 293 K* vs. η *and best linear fits according to* Stokes-Einstein-Debye *hydrodynamics theory* (solid lines). 1. acetonitrile, 2. propionitrile, 3. butyronitrile, 4. valeronitrile, 5. hexanitrile, 6. octanenitrile, 7. dimethylsulfoxide, 8. dimethylformamide, 9. benzonitrile.

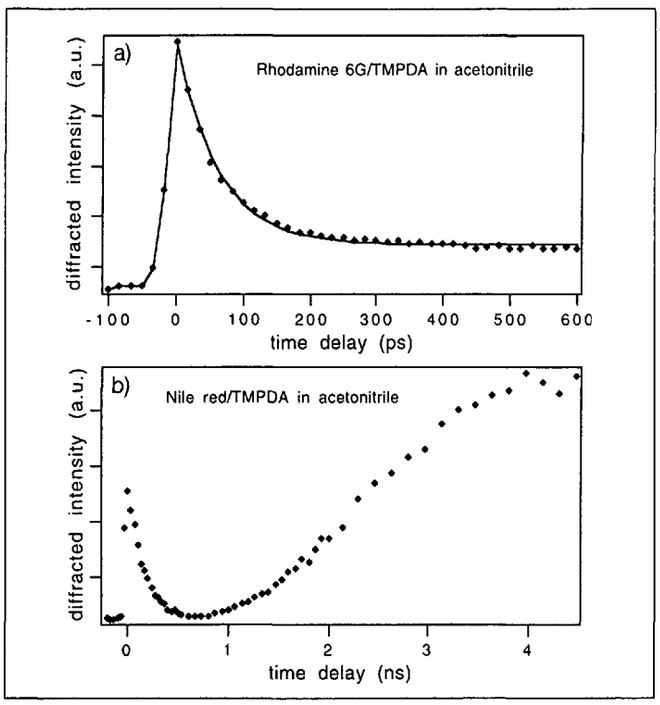

Fig. 5. *Time evolution of the diffracted intensity due to the ground state recovery of* a) Rhodamine 6G *and* b) *Nile red with 0.5M TMPDA in MeCN*

some donor/acceptor systems using time resolved resonance *Raman* spectroscopy [15]. Although the electronic absorption spectrum of the geminate ion pair is the same as that of the free ions, k_{sep} can be estimated from the free ion yield and the rate constant of back-electron transfer, k_{bet} [16].

These two parameters have been determined with the A/D couple *Rhodamine 6G*/TMPDA (*N,N,N',N'*-tetramethylphenylenediamine) in MeCN. In this case, the e.t. takes place from a neutral species to an excited cation to generate a radical cation and a neutral radical [17]. *Fig. 5a* shows the diffracted intensity due to the ground-state recovery of *Rhodamine 6G*. The fast decay is due to the back e.t. within the radical pair and the very slow decay, a plateau at that time scale, corresponds to diffusional recombination of the free radicals. From *Eqns. 3* and *4*, the diffracted intensity is equal to the square of the concentration changes. Therefore, k_{bet} is obtained from the fast decay of the square root of the diffracted intensity and is equal to $1.23 \times 10^{10}\ s^{-1}$. The radical yield, Φ_r, is equal to the square root of the ratio of the diffracted intensity at the plateau to the diffracted intensity at the maximum, *i.e.*, $\Phi_r = 0.53$. The rate constant for the separation can be calculated with these two values, $k_{sep} = \Phi_r k_{bet}/(1-\Phi_r) = 1.39 \times 10^{10}\ s^{-1}$. This is almost 30 times larger than the value reported for the separation of a geminate ion pair [18]. This difference may reflect the effect of the *Coulomb* interaction between two charged ions. Further investigations on the effect of electric charge and molecular size on k_{sep} are in progress.

Finally, *Fig. 5b* shows the diffracted intensity for the ground state recovery of Nile red and TMPDA in MeCN. In this case, the intensity decays very rapidly to almost zero and rises again after a time delay of *ca.* 1 ns. This rise corresponds to the formation of a thermal grating. Most of the absorbed excitation energy is dissipated as heat, causing a local temperature rise, which induces a change of refractive index. The slow rise is due to the acoustic transit time, *i.e.*, the time needed for the heat to propagate. This time is equal to the fringe spacing of the grating divided by the speed of sound in the solvent. To resolve the kinetics of the thermal grating, a large incidence angle, *i.e.*, a small fringe spacing, has to be used. With a pump wavelength of 355 nm, transit acoustic times as short as 100 ps can be obtained in MeCN. This contrasts strongly with the thermal lensing spectroscopy, where the time resolution is limited to several hundreds of ns. To avoid interference between thermal and amplitude gratings, the acoustic transit time can be easily lengthened up to more than 200 ns by using a small incidence angle.

5. Conclusions

The above results show that transient grating spectroscopy is a versatile tool to study the dynamics of photoinduced processes. Although the optical arrangement is more complex than for flash photolysis, this method is more sensitive and requires, therefore, less excitation intensity. Nonradiative transitions can also be investigated by monitoring the light diffracted by thermal gratings with a time resolution that is not achievable with other conventional techniques.

The detection of amplitude gratings is optimal in the ps timescale. In the ns time scale, thermal gratings can interfere, while in the fs time scale nonlinear phenomena depending on the third order nonlinear susceptibility can render the interpretation of the diffracted signal more difficult. However, by varying the polarisations of the two pump and the probe beams, it is possible to separate these different contributions [19].

The authors thank Prof. *P. Suppan* for helpful advices and discussions. *E.V.* thanks Prof. *E. Haselbach* and Prof. *A. von Zelewsky* for their initiative concerning the *programme d'encouragement à la relève universitaire de la Confédération*. This work was supported by the *Fonds national suisse de la recherche scientifique* through project No. 21-36150.92. *A. H.* whishes to thank the *Fonds national suisse de la recherche scientifique* for support through project No. 20-34071.92.

Received: July 6, 1994

[1] C. Bräuchle, D. M. Burland, *Angew. Chem. Int. Ed.* **1983**, *22*, 582.
[2] A. N. Russu, E. Vauthey, C. Wei, U. P. Wild, *J. Phys. Chem.* **1991**, *95*, 10496.
[3] H. J. Eichler, P. Günter, D. W. Pohl, 'Laser-Induced Dynamic Gratings', Springer Verlag, Berlin, 1986.
[4] J. T. Fourkas, M. D. Fayer, *Acc. Chem. Res.* **1992**, *25*, 227.
[5] H. Kogelnik, *Bell System Tech. J.* **1969**, *48*, 2909.
[6] Y. Cui, M. Zhao, G. S. He, P. N. Prasad, *J. Phys. Chem.* **1991**, *86*, 4694.
[7] R. S. Moog, M. D. Ediger, S. G. Boxer, M. D. Fayer, *J. Phys. Chem.* **1982**, *86*, 4694.
[8] E. Vauthey, *Chem. Phys. Lett.* **1993**, *216*, 530.
[9] S. P. Velsko, D. H. Fleming, D. H. Waldeck, *J. Chem. Phys.* **1983**, *78*, 249.
[10] H. F. Grote, J. T. Hynes, *J. Chem. Phys.* **1980**, *73*, 2715.
[11] B. Bagchi, D. W. Oxtoby, *J. Chem. Phys.* **1983**, *78*, 2735.
[12] K. Kalyanasundaram, *Chem. Soc. Rev.* **1978**, *7*, 453.
[13] M. Hasegawa, T. Sugimura, Y. Suzaki, Y. Shindo, A. Kitahara, *J. Phys. Chem.* **1994**, *98*, 2120.
[14] M. P. Pileni, *J. Phys. Chem.* **1993**, *97*, 6961.
[15] E. Vauthey, D. Phillips, A. W. Parker, *J. Phys. Chem.* **1992**, *96*, 7356.
[16] S. M. Hubig, *J. Phys. Chem.* **1992**, *96*, 2903.
[17] E. Vauthey, P. Suppan, *Chem. Phys.* **1989**, *139*, 381.
[18] A. Weller, *Pure Appl. Chem.* **1982**, *54*, 1885.
[19] F. W. Deeg, M. D. Fayer, *J. Chem. Phys.* **1989**, *91*, 2269.